Available online at www.sciencedirect.com
SCIENCE DIRECT
Sensors and Actuators A 104 (2003) 236–245
SENSORS AND ACTUATORS A PHYSICAL
www.elsevier.com/locate/sna

Applications of a low contact force polyimide shank bolometer probe for chemical and biological diagnostics

M.-H. Li, Y.B. Gianchandani*

Department of Electrical and Computer Engineering, Center for NanoTechnology, University of Wisconsin, Madison, WI, USA

Abstract

This paper reports on the detection of nano-scale chemical variations in photosensitive polymers and biological variations in cancerous tumor cells that have been accomplished for the first time using scanning thermal probes that we have developed. It also reports on changes that have been made over older versions of this probe to help achieve these capabilities. The probe is fabricated by a 6-mask surface micromachining process using polyimide as the structural material. A unique assembly sequence that involves flipping over the probe accommodates the future integration of circuitry on the same substrate. The probe has measured spring constant 0.082 N/m for a 250 μm × 50 μm × 3 μm probe. It offers a tip diameter of 50 nm. Probes are used to study exposed but undeveloped photoresist latent images in features of 70 nm, the acid diffusion in chemically amplified photoresist during post exposure bake, and HeLa cells. Lateral spatial resolution of <50 nm, topographic resolution of <1 nm and thermal resolution of <1.2 mK are demonstrated. Wet scanning capability, which widens the possibility of biochemical applications, is also demonstrated for the first time. The structure, fabrication, and assembly of the probe and the interface circuit used for these experiments are described.
© 2003 Elsevier Science B.V. All rights reserved.

Keywords: Polyimide shank; Bolometer; Chemical diagnostics

1. Introduction

Scanning thermal microscopy has been explored for a number of applications, including high resolution temperature mapping, topographical mapping, data storage, photothermal absorption spectroscopy, and subsurface imaging [1–4]. Temperature sensing methods used for scanning probes have included thermocouples, Schottky diodes, bolometers, and bimorphs [1–12]. A bolometer-type element which senses temperature by fractional changes in the electrical resistance provides certain advantages for microcalorimetry applications. In particular, this resistor can be used not only to sense temperature, but to supply heat if adequate current is passed through it. Since the tip temperature is ultimately influenced by the heat flow between the tip and the sample, variations in thermal conductance across the sample can be mapped by this probe. In essence, the device can be used as a spatially localized microcalorimeter [8,13].

We are developing ultra compliant thermal probes (with spring constant <0.1 N/m) for critical applications in ULSI lithography research. These include, specifically, mapping the latent image of exposed but undeveloped photoresist (PR) to measure photo-acid generation and diffusion independently from the developing step [14]. Since they offer sub-surface mapping capability, thermal probes also facilitate studies of intra-cellular features in bio-related research. To fulfill our need for these applications, probes must have a low spring constant to prevent damaging the soft materials, and provide spatial resolution <100 nm. In addition, to permit scanning in aqueous environments, complete electrical insulation is necessary. Wet scans are particularly challenging because of enhanced parasitic thermal losses, the need for complete electrical insulation, and the impact of surface tension on the ultra compliant probes. These requirements can not be fulfilled by using the commercially available wire probe which is made of bent bare wires, and has a high spring constant (5 N/m), limited spatial resolution, and no particular isolation [15].

We have previously reported thermocouple or bolometer probes fabricated by 6- to 7-mask surface micromachining processes using polyimide as the shank material, and the application of these probes for temperature mapping, subsurface imaging, and the measurement of glass transition temperature in photoresists [8,9]. This paper reports on applying these probes to ULSI lithography research,

* Corresponding author. Present address: 1301 Beal Avenue, UM Ann Arbor, MI 48109-2122, USA. Tel.: +1-734-615-6407.
E-mail address: yogesh@umich.edu (Y.B. Gianchandani).

0924-4247/03/$ – see front matter © 2003 Elsevier Science B.V. All rights reserved.
doi:10.1016/S0924-4247(03)00026-8

particularly for mapping the latent image of exposed but undeveloped PR to measure photo-acid generation (PAG) and diffusion independently.[1] Wet scanning capability, which widens the possibility of biochemical applications, is also demonstrated for the first time. This paper also describes changes that have been made to older versions [8,9] of this probe to help achieve these capabilities. In the following text, Section 2 describes the device structure and fabrication process, Section 3 describes the measurement theory, and Section 4 describes experimental results that have been obtained.

2. Structure and fabrication

The basic structure of the probe is similar to that reported in [8,9], with a thin film bolometer sandwiched between two layers of polyimide, forming a cantilever. At one end of the cantilever the metal thin film protrudes through an opening in the lower polyimide layer, where it is molded into a pyramidal tip by a notch that was anisotropically wet-etched into the substrate. The tip and a portion of the probe shank are then released from the substrate by etching an underlying sacrificial layer. The released length is then folded over to extend past the die edge for clearance and held in place by an adhesive (Fig. 1). Typical dimensions of the probes after assembly are 250 μm length, 50 μm width, and 3 μm thickness with Cr/Au (200/2000 Å) for the tip and lead, which provides bolometer resistance of about 60 Ω. This flip-over method for providing the tip clearance exploits the mechanical flexibility of polyimide, and avoids the dissolution of the substrate material from underneath the tip. The polyimide shank offers both high mechanical compliance and high thermal isolation which are important for scanning soft samples with low thermal conductivity, such as PR and polymers.

The present manifestation of the probe (Fig. 2) has an additional thin evaporated film of gold (Cr/Au: 200/5000 Å) that serves as an AFM mirror and also permits a thermo-compression bond to hold the probe after the flip-over step, eliminating the use of epoxy. This method retains the flatness of the probe and significantly increases yield. The released probe was manually flipped over, with the two gold pads (Fig. 2a) held together by using micromanipulators on a hot plate and slowly increasing hot plate temperature to 170 °C. The bonding strength is strong enough. No probe shank bounce back, cracking or breakage has been observed in the many 10s of samples that have been assembled in this manner. Other materials such as using partially curried photosensitive polyimide (PI2721™) or indium were also evaluated, but all show some drawbacks. The partially curried polyimide can be attacked by photoresist stripper, and the indium is attacked by the prolonged HF etching to release the probe tip. Other self-assembly approaches such as using surface tension forces [16] and a bimorph for stress mismatch were also studied, but all fail to retain the flatness of the flipped-over probe due to its fundamental limitation. Typical dimensions of the probes after assembly are 250 μm length, 50 μm width, and 3 μm thickness with Cr/Au (200/2000 Å) for the tip and lead, which have probe resistance about 60 Ω. The probe shank length can be easily adjusted by moving the location of the gold bond pads.

Another critical process step that has been added permits reduction of the tip diameter to about 50 nm by oxide sharpening the tip notch using the phenomena of the non-uniform

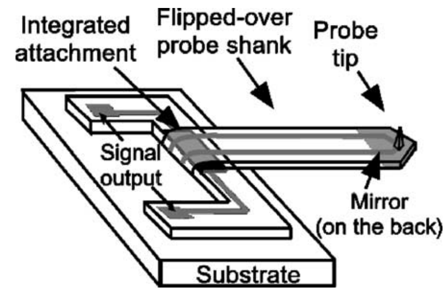

Fig. 1. Schematic of the ultracompliant polyimide thermal probe.

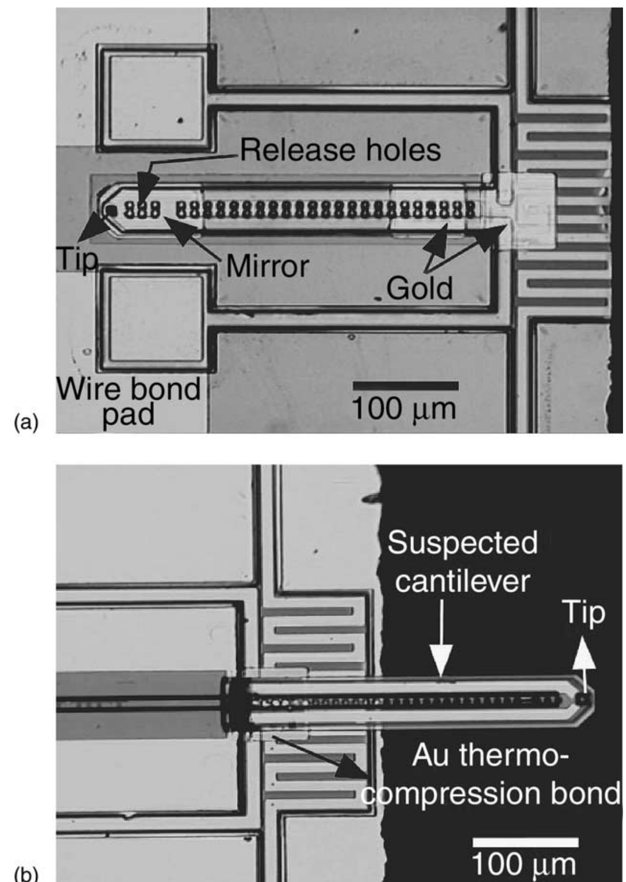

Fig. 2. (a) A scanning thermal probe showing the location of mirror and gold segments for thermocompression bond; (b) a 250 μm long probe flipped over the die edge and held down with a gold thermocompression bond.

[1] Portions of this paper will appear in [12].

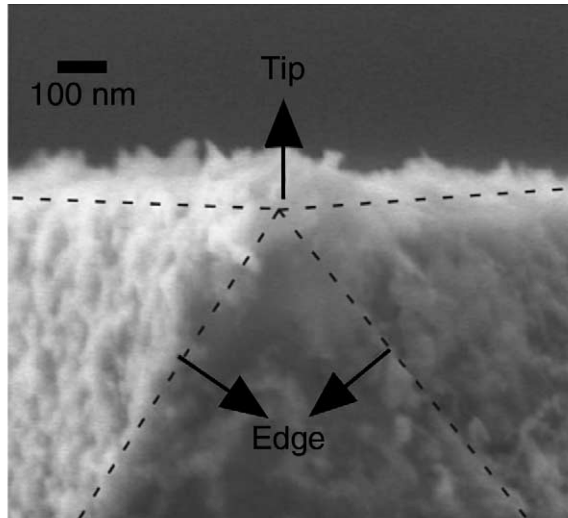

Fig. 3. Close-up of the sharpening tip showing the tip diameter is about 50 nm.

oxide growth [17]. A 4000 Å thick oxide is grown at 950 °C prior to depositing the sacrificial layer used for releasing the probe shank from the silicon substrate, which generates a tip diameter of about 50 nm as shown in Fig. 3.

Since the probe length is only about 300 μm, and the wafer thickness of a 3″ wafer is approximately 500 μm, a small extrusion at the die edge caused by the curvature of the dicing blade can block the laser beam (Fig. 4a). To provide a clear die edge for laser pickup, the probe wafer is bonded to a dummy wafer using photoresist, with the front side of the wafer covered by a thin photoresist film to protect the probes during dicing, and has both wafers diced together as shown in Fig. 4b. A 3″ wafer can generate about one thousand dies with two probes per die.

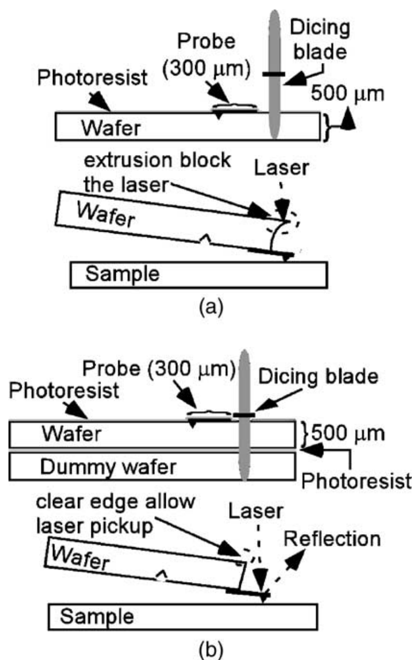

Fig. 4. (a) Extrusion at die edge blocks the laser; (b) with two wafers bonded and diced together to provide a clear die edge after dicing, which allows laser pickup.

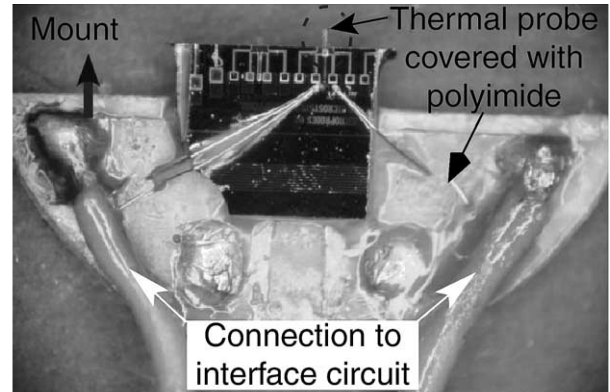

Fig. 5. A mounted scanning thermal probe with the base covered with a polyimide (PI2613^{TM}) layer to make it suitable for working in aqueous environments.

For operation in aqueous environments, the bond pads and bond wires are covered with a thin layer of polyimide (PI2613^{TM}), leaving the scanning tip as the only exposed metallic surface (Fig. 5). The polyimide probe provides high thermal probe shank resistance, low spring constant, and an integrated tip. These advantages make it suitable to study soft materials such as chemical amplified photoresist for deep-UV lithography and HeLa tumor cells.

3. Measurement theory

3.1. Interface circuit

Fig. 6 shows an interface circuit used to sense the probe resistance change as it scans across the sample surface. It includes a Wheatstone bridge, two gain stages providing combined amplification of 10^4, and a low-pass filter with a cutoff frequency of 1 kHz to reduce noise. The output voltage (V_{out}) is plotted for the thermal image.

When the probe resistance change (ΔR_P) is much smaller than the probe resistance (R_P), as in the case of thermal

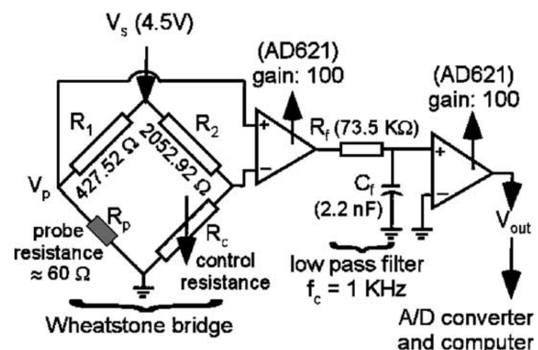

Fig. 6. An interface circuit for sensing the probe resistance change.

conductance contrast mapping, the output voltage change (ΔV_{out}) can be expressed as:

$$\Delta V_{out} \cong 10^4 \times V_s \times \Delta R_P \frac{R_1}{(R_1 + R_P)^2} \quad (1)$$

where V_s is the voltage applied to the Wheatstone bridge, and R_1 is a resistance of the Wheatstone bridge as shown in Fig. 6. The supplied power change (ΔP_p) of the probe resistor due to the probe resistance change (ΔR_P) is:

$$\Delta P_p \cong \frac{V_P^2}{R_P}\left(\frac{\Delta R_P (R_1 - R_P)}{R_P (R_1 + R_P)}\right) \quad (2)$$

According to Eqs. (1) and (2), the output voltage change (ΔV_{out}) is linearly proportional to the supplied power change (ΔP_p). Since the supplied power change (ΔP_p) is equal to the conductive heat loss between the tip and sample, which is proportional to change in the thermal conductance of the sample, the output voltage change (ΔV_{out}) represents the thermal conductance contrast of sample.

The probe tip temperature change (ΔT_P) can be calculated from the output voltage change (ΔV_{out}), which is:

$$\Delta T_P \cong \frac{\Delta V_{out} (R_1 + R_P)^2}{(10^4 V_s R_1 R_P \mathrm{TCR})} \quad (3)$$

The temperature coefficient of resistance (TCR) is 3640 ppm/K for Cr/Au (200/2000 Å) thin film. A ΔV_{out} of 100 mV corresponds to a ΔT_P of 5.657 mK calculated using the voltage and resistance values shown in Fig. 6. The full scale ΔT_P is indicated for all thermal scans presented in this paper. Before a scan, this circuit is adjusted to balance the Wheatstone bridge with the probe in contact with the sample by adjusting the control resistor (R_c) to make the resistance ratio of R_c/R_2 equal to R_P/R_1 so that the output voltage is as close as possible to 0 V in order to make full use of the available dynamic range.

3.2. Thermal conductance contrast mapping

When the probe is operated at a constant tip temperature (T_P), and with the sample thickness sufficiently thick compared with the tip diameter, the heat loss (P_s) to the sample can be expressed as [4]:

$$P_s = \frac{2\pi k_s a (T_P - T_0)}{1 + (2\pi k_s a R_g)} \quad (4)$$

The heat loss depends on the contact radius a, the ambient temperature T_0, and the tip-sample thermal contact resistance R_g, as well as the sample conductivity k_s. Assuming that the contact area and the tip-sample contact resistance do not change during a scan, the heat loss is then directly proportional to the sample thermal conductivity; i.e. for the image mapped to depend primarily on the sample thermal conductivity, it is necessary that $2\pi k_s a R_g \ll 1$. This requirement can be satisfied for a commercially available wire probe with tip diameter in the range of 1 μm when scanning samples with low thermal conductivity. For the polyimide probe, which has tip diameter ≈50 nm, this constraint is satisfied for virtually any case. Note that under this constraint the thermal probe can even be used to directly measure the sample thermal conductivity, since the supplied power will be directly proportional to it [18,19].

For the case of scanning an ultra-thin photoresist patterned on a silicon wafer with thickness comparable to the scan tip diameter, the heat transfer (P_s) between the probe tip and substrate can be modeled as heat flow through a cylinder:

$$P_s = \frac{(T_P - T_0) A_0 k_s}{H} \quad (5)$$

where T_P is the probe tip temperature, A_0 the tip-sample contact area, k_s the thermal conductivity of photoresist, and H the photoresist thickness. The silicon substrate is a large heat sink, effectively with a fixed temperature T_0. The thermal conductance image obtained from V_{out}, which depends on the heat flow (P_s), contains both topographic image and thermal conductivity information. To separate the influence of topographic variation from (V_{out}), both of the topographic and thermal images should be obtained simultaneously. The topographic image is produced by monitoring the deflection of the probe cantilever as in a conventional AFM by reflecting a laser beam from a mirror placed on the end of cantilever.

4. Measurement results

4.1. Spring constant and spatial resolution

The spring constant (k) is calculated by measuring the thermal fluctuations of the cantilever in the range of 5–25 kHz with the tip suspended 1 μm away from the sample surface using a built-in function in the Topometrix system [20–23]. The spring constant is given by:

$$k = \frac{a k_b T}{P_n} \quad (6)$$

where a is a correction factor (≈0.82), k_b the Boltzmann constant, T the ambient room temperature, and P_n the area of the power spectrum of the thermal fluctuations of the cantilever. The measured spring constant is 0.082 N/m for a 250 μm × 50 μm × 3 μm probe. Since the thermal fluctuations of the cantilever is measured by monitoring the tip motion using the optical-level method of an AFM, and only the fundamental mode of the thermal fluctuation of the cantilever is detected, the correction factor a is 0.82 [22,23]. If all the thermal fluctuation modes are detected, the value of the correction factor a will be 4/3. Another measurement is used to verify the linearity of the force-deflection response of the probe (Fig. 7). The force conversion is determined from the sensor response and the spring constant.

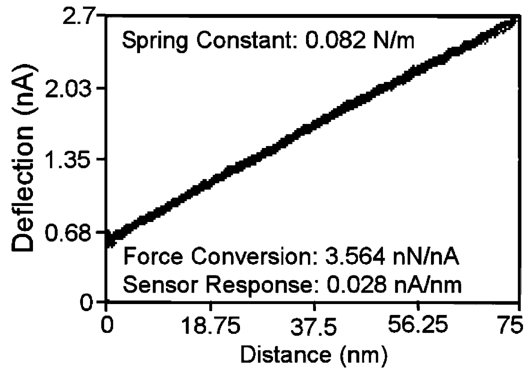

Fig. 7. The measured cantilever deflection versus the piezo displacement of a $250\,\mu m \times 50\,\mu m \times 3\,\mu m$ probe. The cantilever deflection is represented in current, since it is determined by the photosensor response (PSPD).

Fig. 8 shows the scan results for same photoresist sample with z-direction feedback. The topographic image which uses the laser, and the thermal image which uses the resistor were obtained at the same time. The photoresist pattern is 350 nm thick, with trench of 500 nm wide in 2 μm pitch. The low spring constant allows scanning soft material such as photoresist pattern with feature size of 500 nm easily even without z-direction feedback (Fig. 9). The output voltage drops as the probe scanned across the higher thermal conductivity material (silicon), because the heat loss from the tip to sample increases, which cools down the

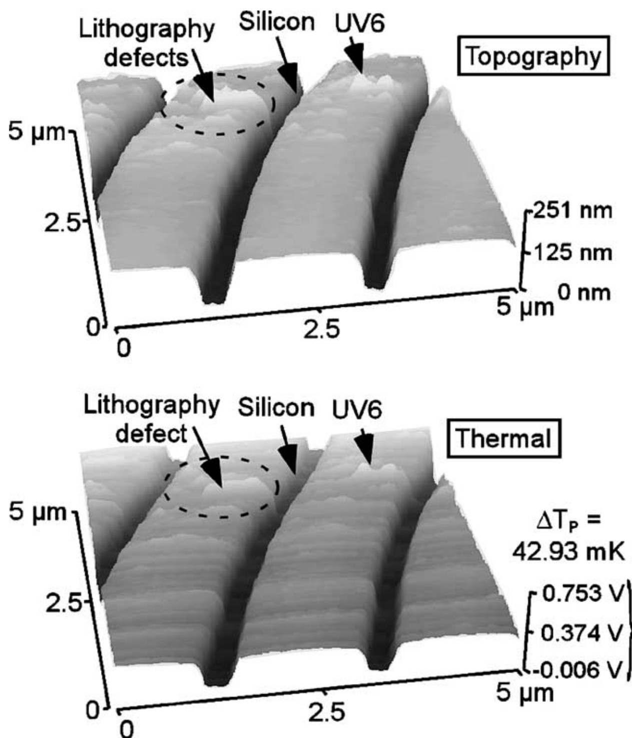

Fig. 8. Topographic (top) and thermal (bottom) images of developed UV6™ photoresist sample with thickness of 350 nm obtained with z-direction feedback.

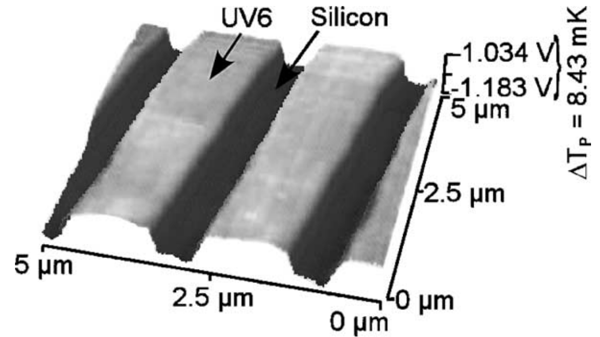

Fig. 9. Thermal image of the same photoresist sample of Fig. 8. No z-direction feedback.

tip temperature, and the corresponding probe resistance. It should be noted that in the absence of feedback control, topographic variations on the sample surface would cause variations in the tip-sample contact force which can potentially affect the image.

Fig. 10 shows the topographic and thermal images of exposed but undeveloped contact hole patterns in Shipley UV113™ photoresist patterned with critical dimension of 70 nm with 200 nm pitch. The images were obtained with scan rate of 0.75 μm/s and resolution of 400 lines. The thermal probe and interface circuit are sensitive enough to detect a photoresist thickness change only 4 nm, which corresponds to a tip temperature change as low as 1.13 mK. Comparing the topographic and thermal images of another photoresist sample shown in Fig. 11, the scan results clearly indicate the probe has spatial resolution of <50 nm, which is comparable to the smallest currently reported. The topographic resolution is <1 nm.

4.2. Photoresist chemistry

The positive tone chemically amplified photoresist UV6™ by Shipley, which is suitable for ultra-narrow line-widths ULSI lithography research, behaves as shown in Fig. 12 [24,25]. Unlike standard PR and PMMA, a photo-acid generated by exposure permits catalyzed thermolysis of the backbone polymer during the post exposure bake (PEB), which changes the solubility of the exposed regions of the

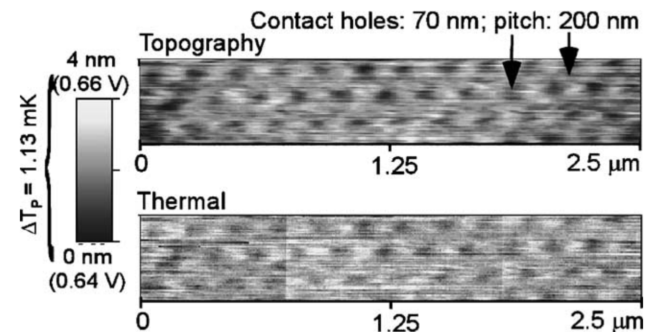

Fig. 10. Topographic (top) and thermal (bottom) images of exposed but undeveloped UV113™ photoresist contact holes of 70 nm.

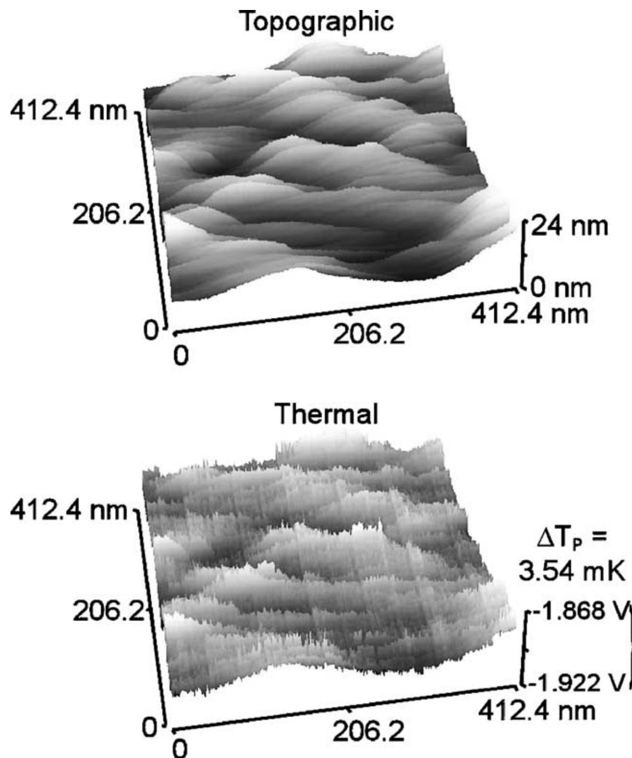

Fig. 11. Topographic (top) and thermal (bottom) images of partial developed UV113™ photoresist sample show the thermal probe has spatial resolution of sub-50 nm.

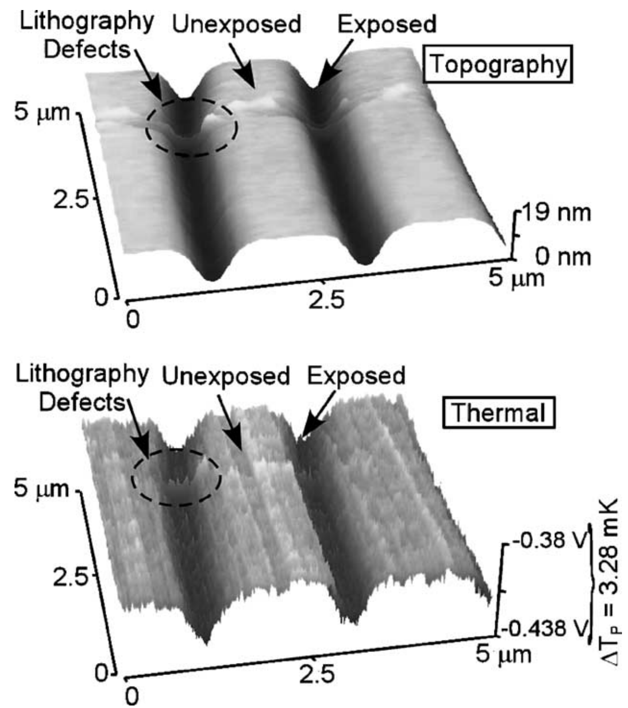

Fig. 13. Both of topographic and thermal images of exposed but undeveloped photoresist-UV6™ of 500 nm thick on 4″ Si wafer obtained simultaneously. Sample was exposed by e-beam with charge density of 9 μC/cm^2, and then post exposure baked at 130 °C for 4 min.

resist and releases isobutylene. The photoresist thickness decreases in exposed areas where the released isobutylene is evaporated during PEB. Topographic variations and thermal conductance variations due to the thermolysis of the backbone are mapped simultaneously by using the thermal probe.

Fig. 13 shows the scan results of a 500 nm thick exposed but undeveloped UV6™ on a 4″ silicon wafer. The sample was exposed using a Leica Cambridge 10.5 EBMF 30 kV electron beam lithography system with charge density of 9 μC/cm^2, and then post exposure baked at 130 °C for 4 min. As discussed previously, in chemically amplified photoresist, the photoresist backbone is cleaved during PEB with an accompanying loss in free volume due to the releasing of isobutylene in the exposed area. The resulting change in thickness combined with the chemical change causes the output voltage to drop as shown in the thermal image. The ‘‘v’’ shape profile shown in the exposed area is due to the dose distribution of the e-beam source [14]. The small lithography defects shown both on the topographic and thermal images clearly indicate the high spatial resolution and sensitivity of thermal probe.

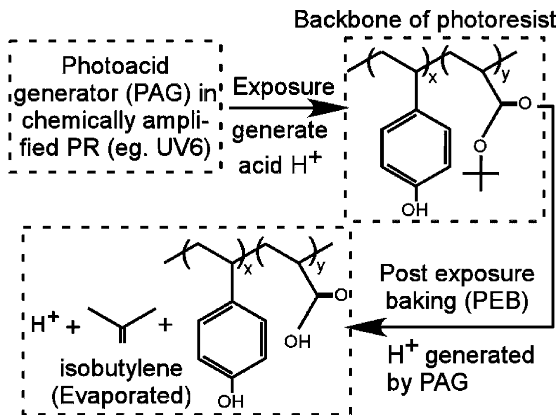

Fig. 12. The mechanism of chemically amplified photoresist UV6™. PAG acid deprotects the backbone during PEB for subsequent dissolution in the developer.

As discussed previously, a post exposure bake is usually required to activate the catalytic reactions. During PEB, acid generated by exposure diffuses and can cause pattern size changes [14,26,27]. It is therefore important to control the PEB conditions to suppress the acid diffusion for the critical dimension control of nanofabrication when using chemical amplification resist systems. Fig. 14 shows the topographic and thermal line scans of a trench in exposed but undeveloped Shipley UV6™ photoresist with different duration of PEB times. As the duration of the 130 °C PEB increases from 45 to 360 s, both the topographic height change (Δh) and ΔV_{out} increase. However, the most significant change in Δh occurs in the 45–90 s period, whereas the most significant change in ΔV_{out} occurs in the 180–360 s period. As noted above, the Δh is due to the release of isobutylene and depends on the acid concentration and the reaction rate of photoresist backbone deprotection. The ‘‘v’’ shape profiles of exposed regions are due to the Gaussian distribution of the e-beam source of dose profile, and hence, the acid

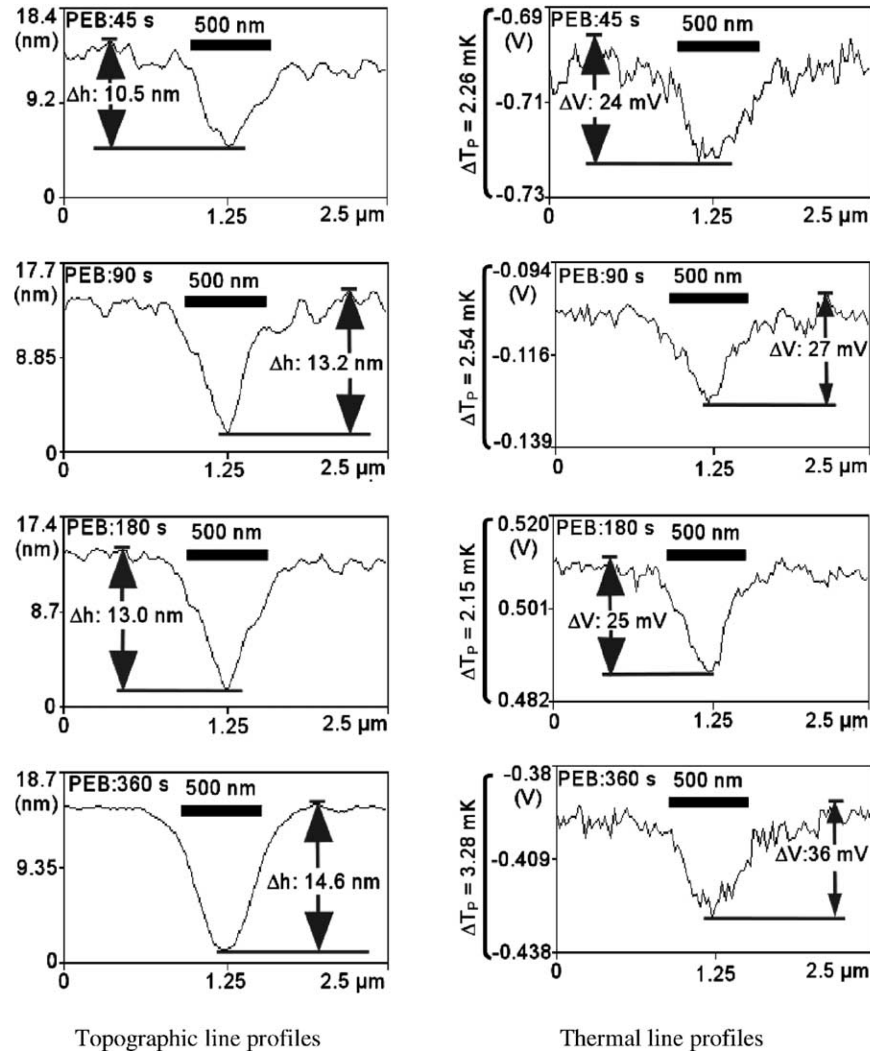

Fig. 14. Topographic (left) and thermal (right) line profiles across the exposed photoresist trench with sample of different post exposure bake time. Both of the topographic height change (Δh) and thermal voltage change (ΔV) increase as the PEB time increases.

concentration [14]. As the PEB time increases, the "v" shape profile widens due to the acid diffusion. However, since the acid diffusion constant, which depends on the process conditions [28], is only about of 50 nm^2/s for UV6™ [26], this change is very small (∼10 nm) [29], particularly when compared to the 500 nm width of the exposed portion. Since the recommended PEB condition for 130 °C is 90 s, the longer PEB times may deplete the photoresist backbone, minimizing subsequent changes in topography. In contrast, other chemical changes may lead to the ΔV_{out} increase during the 180–360 s period.

4.3. Biological analysis

A eukaryotic cell contains many membrane-limited compartments knows as organelles (mitochondrion, lysosome, etc.) separated by the cytoplasm, and a nucleus bounded by a double membrane. The organelles have different cellular functions, and have slightly different thermal conductivity compared with that of cytoplasm. In addition, the temperatures of some organelles are expected to be different. For example, the mitochondria are the energy generators of the cell. Therefore, the temperature at the mitochondria should be higher. The thermal probes are capable of mapping both thermal conductance and temperature variations. Since subsurface variations in these quantities can be detected while the topography is being mapped as well, the thermal probes can potentially be useful tools for studying cellular activity under different conditions. The low spring constant (0.082 N/m), the high thermal isolation, and high spatial resolution (<50 nm) of the polyimide probes are important assets in this kind of application. Here, we demonstrated the usage of applying the thermal probe to map the thermal conductance contrast of fixed HeLa tumor cells, which are widely used for studying cellular functions [30]. These cells typically have a diameter of about 30 μm, with a very large nucleus. The optical, topographic and thermal images of the nucleus of a HeLa cell fixed to a glass slide while undergoing

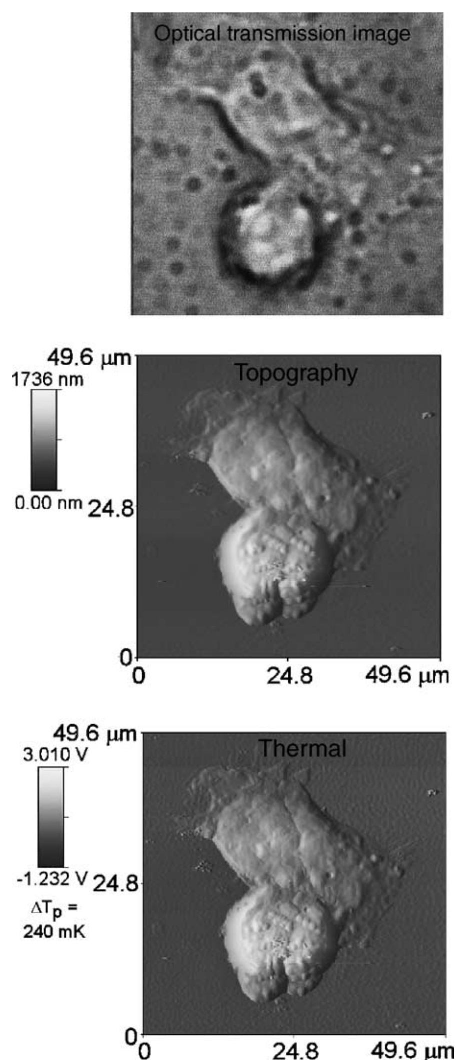

Fig. 15. The optical, topographic and thermal images of the nucleus of a HeLa cell fixed to a glass slide while undergoing mitosis. The optical image was obtained from transmission microscopy. The topographic and thermal images obtained from thermal probes are almost identical since the probe tip heat loss due to topographic change is dominant.

mitosis are compared in Fig. 15. The optical image was obtained using transmission microscope (Axiovert 100TV) with samples in the microscope immersion oil. Since the topographic variation in such a sample is much larger than the thermal conductivity difference of the organelles within it, the thermal image is expected to be similar to the topography map. The distinctions between these images are evidence of variations in subsurface conductivity.

4.4. Scanning in aqueous environments

Aqueous scans are particularly challenging because of enhanced parasitic thermal losses between the probe shank and substrate, the need for complete electrical insulation, and the impact of surface tension on the ultra compliant probes. The probe and mounting platform must be immersed in the liquid along with the sample to circumvent the surface

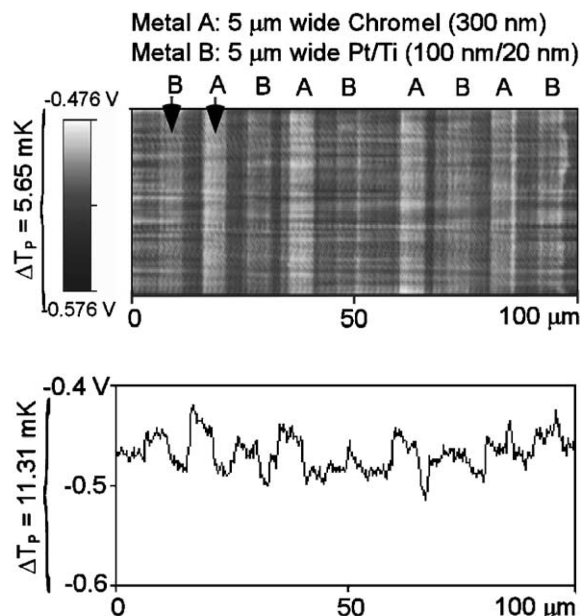

Fig. 16. Area (upper) and line scan (lower) thermal images of metal stripes on a Si substrate obtained without z-direction feedback with the probe and sample immersed in water.

tension forces, and to provide a uniform surrounding environment. The spatial resolution and temperature sensitivity degrade due to the parasitic thermal liquid conductance between the probe shank and sample. Since the liquid (~1 W/m K) has much higher thermal conductivity than that of air (2.6×10^{-2} W/m K), the heat transfer between the probe shank and sample substrate can no longer be neglected.

Fig. 16 presents area and linear thermal scans of metal lines on a Si substrate in an aqueous environment. The sample was 5 µm wide thin film chromel (metal A: 300 nm thick), and Ti/Pt (metal B: 20/100 nm thick) patterned on a Si substrate and isolated from it by a 0.75 µm thick silicon dioxide layer. The variation in metal films is clearly detectable despite the fact that these scans were performed without z-axis feedback. This is possible because of the ultra compliant nature and high thermal isolation offered by the probe. We believe this is the first scanning thermal probe that can work in aqueous environment. With the ability of scanning in aqueous environments, these probes can potentially facilitate studies of cellular features and functions of living cells in real time to provide other information not provided by AFM, such as the temperature distribution in a cell that is undergoing mitosis.

4.5. Performance analysis

Table 1 shows the current performance of polyimide thermal probe with the interface circuit. The probe has tip diameter about 50 nm, and spatial resolution of sub-50 nm as shown in Figs. 4 and 11 respectively. According to Fig. 14, the thermal probe can easily detect output voltage changes

Table 1
Current performance of polyimide thermal probe with the interface circuit

Tip diameter (nm)	≈50
Lateral spatial resolution (nm)	<50
Topographic resolution (nm)	<1
Input referred circuit noise (1 kHz BW) (μV)	<2
ΔR resolution (mΩ)	<0.25
Tip temperature resolution (mK)	<1.2
Detectable thermal conductance change (W/K) (1%)	1×10^{-11}
Detectable thermal conductivity change (W/m K) (1%)	2×10^{-3}

lower than 20 mV. Since interface circuit has voltage gain of 10^4, this indicates the interface circuit can detect input signal change lower than 2 μV. Calculated using Eqs. (1) and (3), this also indicates the interface circuit can sense 0.25 mΩ probe resistance change or 1.2 mK temperature change in the probe temperature.

Comparing the line profiles of topographic and thermal scan at unexposed area in Fig. 13, it shows the thermal probe can easy detect photoresist thickness change lower than 1% (5 variation of 500 nm thick). Since the output voltage is proportional to the thermal conductance between the tip and silicon substrate, which is k_sA_0/H as discussed at Eq. (5), it implies the thermal probe can also detect thermal conductance change lower than 1%, which is 1.09×10^{-11} W/K (1% of k_sA_0/H) by assuming that the tip-sample contact area (A_0) is $30^2\,\pi$ nm^2, and the thermal conductivity of photoresist (k_s) is comparable to that of PMMA (0.193 W/m K) [2]. By the same argument, the thermal probe can also detect the thermal conductivity changes lower than 1%, which is 1.93×10^{-3} W/m K.

5. Conclusion

This effort has addressed the development and applications of a polyimide shank thermal probe fabricated by a 6-mask surface micromachining. These probes are assembled with the help of a thermocompression bond between thin films that greatly improved yield. A modification of the structure permits operation in aqueous environments. Typical probe dimensions are 250 μm length, 50 μm width, and 3 μm thickness. The probe is ultra-compliant with a spring constant of 0.082 N/m, and can be further reduced by reducing the probe width and thickness. It can be operated without z-direction feedback, even when scanning soft materials.

The probe has a lateral spatial resolution of sub-50 nm, and a topographical resolution of <1 nm. Combined with the interface circuit, the probe can offer tip temperature resolution better than 1.2 mK. The probe has been used to scan exposed but undeveloped photoresist samples, HeLa cells, and to study the acid diffusion in photoresist during post exposure bake. A sample scanned with both of probe and sample immersed in water is also presented. These results suggest the potential usefulness of the polyimide probe as a tool for measuring the cellular activity of living cells in aqueous environments.

Acknowledgements

The authors thank Prof. Cerrina and Dr. Leo Ocola for supporting the photoresist samples, and Prof. Menon and Dr. Vainauskas for providing HeLa cell samples. This work was funded in part by the Semiconductor Research Corporation contract # 98-LP-452.005. The Center for NanoTechnology, University of Wisconsin-Madison, is supported in part by DARPA/ONR grant # MDA 972-00-1-0018, and # MDA 972-99-1-0013. The Synchrotron Radiation Center, University of Wisconsin-Madison, at which some of the experimental facilities are located, is operated under NSF award # DMR-0084402.

References

[1] H.K. Wickramasinghe, Scanned-Probe Microscopes, Scientific American, 1989, pp. 98–105.
[2] A. Hammiche, D.J. Hourston, H.M. Pollock, M. Reading, M. Song, Scanning thermal microscopy: subsurface imaging, thermal mapping of polymer blends, and localized calorimetry, J. Vac. Sci. Technol. B 14 (2) (1996) 1486–1491.
[3] P. Vettiger, M. Despont, U. Drechsler, U. Dürig, W. Häberle, M.I. Lutwyche, H.E. Rothuizen, R. Stutz, R. Widmer, G.K. Binnig, The millipede-more than one thousand tips for future AFM data storage, IBM J. Res. Develop. 44 (3) (2000) 323–340.
[4] A. Majumdar, Scanning thermal microscopy, Annu. Rev. Mater. Sci. 29 (1999) 505–585.
[5] Y. Suzuki, Novel microcantilever for scanning thermal imaging microscopy, Jpn. J. Appl. Phys. Part 2 35 (3A) (1996) L352–L354.
[6] Y.B. Gianchandani, K. Najafi, A silicon micromachined scanning thermal profiler with integrated elements for sensing and actuation, IEEE Trans. Electron Dev. 44 (11) (1997) 1857–1867.
[7] T. Leinhos, M. Stopka, E. Oesterschulze, Micromachined fabrication of Si cantilevers with Schottky diodes integrated in the tip, Appl. Phys. A 66 (1998) S65–S69.
[8] M.-H. Li, Y.B. Gianchandani, Microcalorimetry applications of a surface micromachined bolometer-type thermal probe, J. Vac. Sci. Technol. B 18 (6) (2000) 3600–3603.
[9] M.-H. Li, J.J. Wu, Y.B. Gianchandani, Surface micromachined polyimide scanning thermocouple probes, J. Microelectromech. Syst. 10 (1) (2001) 3–9.
[10] D.-W. Lee, T. Ono, T. Abe, M. Esashi, Fabrication of microprobe array with sub-100 nm nano-heater for nanometric thermal imaging and data storage, in: Proceedings of the 11th International Conference On Solid-State Sensors and Actuators (Transducers '01), June 2001, pp. 204–207.
[11] L. Shi, O. Kwon, A.C. Miner, A. Majumdar, Design and batch fabrication of probes for sub-100 nm scanning thermal microscopy, J. Microelectromech. Syst. 10 (3) (2001) 370–378.
[12] M.-H. Li, J.-H. Lee, F. Cerrina, A.K. Menon, Y.B. Gianchandani, Chemical and biological diagnostics using fully insulated ultra-compliant thermal probes, in: Proceedings of the Hilton Head 2002, Solid-State Sensor, Actuator, and Microsystems Workshop, 2–6 June 2002.
[13] D. Fryer, P. Nealey, J. de Pablo, Thermal probe measurements of the glass transition temperature for ultrathin polymer films as a function of thickness, Macromolecules 33 (17) (2000) 6439–6447.

[14] L.E. Ocola, D. Fryer, P. Nealey, J. dePablo, F. Cerrina, S. Kämmer, Latent image formation: nano-scale topography and calorimetric measurements in chemical amplified resists, J. Vac. Sci. Technol. B 14 (6) (1996) 3974–3999.
[15] TM Microscopes, http://www.tmmicro.com, Probe Model no. 1615-00.
[16] R.R.A. Syms, Equilibrium of hinged and hingeless structures rotated using surface tension forces, J. Microelectromech. Syst. 4 (4) (1995) 177–184.
[17] S. Akamine, C.F. Quate, Low temperature thermal oxidation sharpening of microcast tips, J. Vac. Sci. Technol. B 10 (5) (1992) 2307–2310.
[18] F. Ruiz, W.D. Sun, F.H. Pollak, C. Venkatraman, Determination of the thermal conductivity of diamond-like nanocomposite films using a scanning thermal microscope, Appl. Phys. Lett. 73 (13) (1998) 1802–1804.
[19] D.I. Florescu, V.M. Asnin, F.H. Pollak, A.M. Jones, J.C. Ramer, M.J. Schurman, I. Ferguson, Thermal conductivity of fully and partially coalesced lateral epitaxial overgrown GaN/sapphire (0001) by scanning thermal microscopy, Appl. Phys. Lett. 77 (10) (2000) 1464–1466.
[20] J.L. Hutter, J. Bechhoefer, Calibration of atomic-force microscope tips, Rev. Sci. Instrum. 64 (7) (1993) 1868–1873.
[21] Topometrix Corporation, User's Manual Supplement, SPMLab Version 3.06, 1995, pp. 2–19s.
[22] J. Bechhoefer, J.L. Hutter, unpublished.
[23] H.-J. Butt, M. Jaschke, Calculation of thermal noise in atomic-force microscopy, Nanotechnology 6 (1995) 1–7.
[24] R.D. Allen, W.E. Conley, R.R. Kunz, Deep-UV resist technology, in: P. Rai-Choudhury (Ed.), Handbook of Microlithography, Micromachining and Microfabrication, vol. 1, Microlithography, SPIE, Bellingham, Washington, 1997.
[25] H. Ito, Chemically amplified resists: past, present, and future, SPIE 3678 (1999) 2–12.
[26] D. Kang, E.K. Pavelchek, C. Swible-Keane, The accuracy of current model descriptions of a DUV photoresist, SPIE 3678 (1999) 877–890.
[27] T. Yoshimura, T. Nakayama, S. Okazaki, Acid-diffusion effect on nanofabrication in chemical amplification resist, J. Vac. Sci. Technol. B 10 (6) (1992) 2615–2619.
[28] T. Itani, H. Yoshino, S. Hashimoto, M. Yamana, N. Samoto, K. Kasama, A study of acid diffusion in chemically amplified deep ultraviolet resist, J. Vac. Sci. Technol. B 14 (6) (1996) 4226–4228.
[29] T.H. Fedynyshyn, J.W. Thackeray, J.H. Georger, M.D. Denison, Effect of acid diffusion on performance in positive deep ultraviolet resists, J. Vac. Sci. Technol. B 12 (6) (1994) 3888–3894.
[30] R.L. Warters, O.L. Stone, Histone protein and DNA synthesis in HeLa cells after thermal shock, J. Cell. Phys. 118 (1984) 153–160.